

# Controlled Functionalization of Carbonaceous Fibers for Asymmetric Solid-State Micro-Supercapacitors with High Volumetric Energy Density

Dingshan Yu, Kunli Goh, Qiang Zhang, Li Wei, Hong Wang, Wenchao Jiang, and Yuan Chen\*

The rapid advances in miniaturized consumer electronics and micro-electromechanical systems require high-performance energy storage system with a small volume (i.e., high volumetric energy and power density).<sup>[1–4]</sup> Micro-supercapacitors (micro-SCs) with a size of tens to hundreds of micrometers are promising energy storage systems for miniaturized devices because of their excellent rate capability, high power density, and long lifetime.<sup>[2–4]</sup> Different from conventional two-dimensional (2D) planar device architectures, fiber micro-SCs based on fibrous/interwoven substrates can be directly used as wearable components in textile/fabric electronics. A few types of carbonaceous fibers, such as carbon fibers,<sup>[7,8]</sup> reduced graphene oxide (rGO) fibers,<sup>[9]</sup> single-walled or multi-walled carbon nanotube (SWCNT or MWCNT) fibers,<sup>[10–12]</sup> or carbon-based composite fibers containing pseudocapacitive materials,<sup>[13–17]</sup> are particularly attractive for fiber-based micro-SCs due to their one-dimensional (1D), flexible, and conductive features. Despite the recent progress in fiber-based micro-SCs, a key challenge is to increase their energy density without sacrificing their lifetime and power density.

The energy density ( $E$ ) of micro-SCs is determined by the equation  $E = C_{cell}V^2/2$ , where  $C_{cell}$  is the cell capacitance,  $V$  is the operating voltage. Thus, the energy density could be improved by either developing high-capacitance electrode materials or increasing the cell voltage. It is attractive to have high-voltage micro-SCs, which can not only improve the energy density, but also reduce the number of devices needed in series for high voltage applications. Unfortunately, most reported fiber-based micro-SCs are based on symmetric device configuration with two identical fiber electrodes, and their operating voltage is limited to 0.8–1 V.<sup>[7–17]</sup> A promising strategy to achieve both wide voltage window and high energy density is to construct

asymmetric micro-SCs with one capacitor-type electrode as power source and the other battery-type Faradic electrode as energy source.<sup>[5,6]</sup> This renders different electrochemical windows of two types of electrodes to achieve a high working voltage, and thus could lead to an improved energy density. We envision that three key tasks to obtain high energy density in asymmetric SCs are: (1) to design suitable capacitive electrode materials (usually carbon materials); (2) to select proper Faradic electrode materials (usually nanostructured pseudocapacitive materials); and (3) to balance the charges ( $q = C_m m \Delta E$ ) stored in two active electrodes ( $q^+ = q^-$ ), where  $C_m$  is the gravimetric capacitance of the electrode material,  $m$  is the mass of electrode,  $\Delta E$  is the applied potential difference for the charge/discharge process.<sup>[6]</sup>

The asymmetric SC design has been demonstrated in conventional macroscale SCs, which usually employ a sandwich structure consisting of two different thin-film electrodes with carbon materials as negative electrodes and metal oxides (e.g.,  $\text{MnO}_2$ ) or metal hydroxide (e.g.,  $\text{Ni}(\text{OH})_2$ ) as positive electrodes.<sup>[5,6,18–20]</sup> The active electrode materials in the positive and negative electrodes are synthesized in bulk powder forms, and the charge balance in macro-scale devices can be achieved by adjusting the mass ratio of the active materials in the two electrodes. In contrast, the design and fabrication of flexible fiber-based asymmetric micro-SCs are more difficult because: (1) the synthesis of electrode materials in fibers is constrained by the fiber geometry and mechanical flexibility requirements; (2) most of pseudocapacitive materials used as Faradic electrodes in macro-scale SCs cannot be fabricated into flexible fiber electrodes, limiting the choices of Faradic electrode materials; (3) the decrease in size of micro-SCs implies a diminishing amount of active materials in each fiber electrode. Thus, it is hard to reach charge balance in the two electrodes by simply adjusting their mass. Due to the aforementioned difficulties, there are few studies on high voltage asymmetric fiber micro-SCs reported so far. We consider that a critical mission to address these difficulties is to develop versatile fiber electrode materials with tunable capacitances while retaining desirable geometry structure and mechanical flexibility. We recently developed a hydrothermal method using capillary silica column as 1D micro-reactor to synthesize nitrogen-doped rGO/SWCNT fibers in the presence of ethylenediamine (EDA); however, these fibers were only used for fabricating symmetric micro-SCs with the working voltage limited to 1.0 V.<sup>[21]</sup>

In this study, with the aim of designing and assembling highly-efficient asymmetric fiber micro-SCs, we hydrothermally

Dr. D. Yu, Mr. K. Goh, Dr. L. Wei, Dr. H. Wang,  
Mr. W. Jiang, Prof. Y. Chen  
School of Chemical and Biomedical Engineering  
Nanyang Technological University  
62 Nanyang Drive, 637459, Singapore  
E-mail: chenyan@ntu.edu.sg

Prof. Q. Zhang  
Beijing Key Laboratory of Green Chemical Reaction  
Engineering and Technology  
Department of Chemical Engineering  
Tsinghua University, No.1  
Tsinghuayuan, Beijing 100084, P. R. China



DOI: 10.1002/adma.201403061

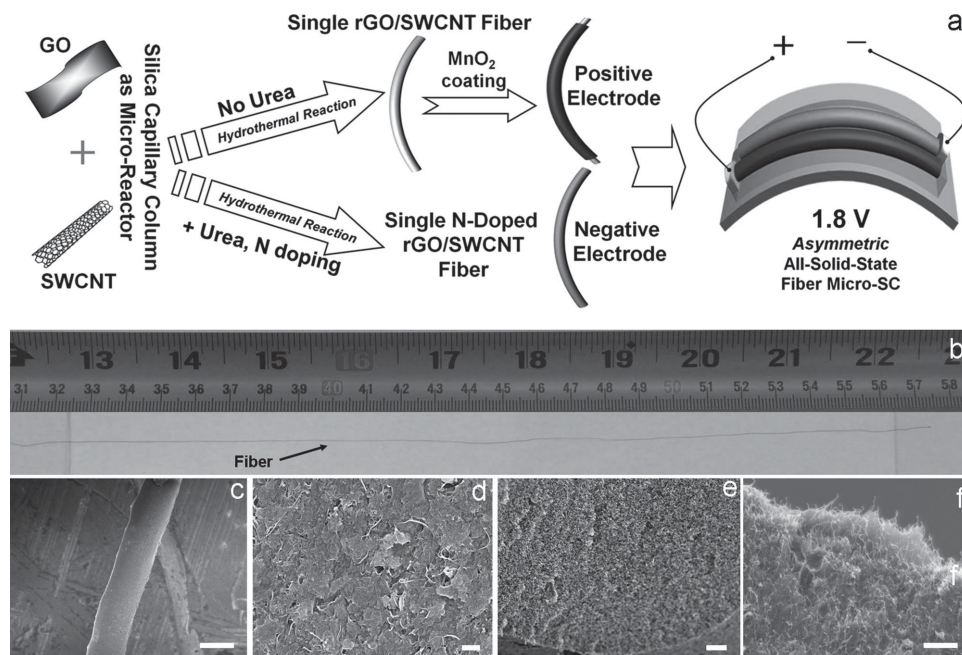


**Figure 1.** (a) Schematic illustration of the design and fabrication of the asymmetric fiber-based micro-SC; (b) The photograph of a 26 cm-long rGO/SWCNT (GCF) all-carbon fiber; (c–f) SEM images of the GCF fiber: (c) overview, (d) surface, (e) cross-section, and (f) fractured end. Scale bars: 50  $\mu\text{m}$  for (c), 100 nm for (d), and 1  $\mu\text{m}$  for (e) and (f).

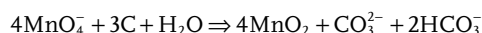
synthesized a new undoped rGO/SWCNT all-carbon fiber, and judiciously utilized it as an effective platform, which enables controllable functionalization through a facile route to yield versatile carbon composite fibers with either capacitive or Faradic characteristics. The capacitive-type fibers were obtained by in-situ doping nitrogen into the rGO/SWCNT fiber using urea as the nitrogen precursor during hydrothermal synthesis, while the Faradic-type fibers were created by redox deposition of  $\text{MnO}_2$  on the rGO/SWCNT fibers at ambient conditions. Both functionalized fibers show greatly enhanced capacitive performances, which can be further tuned by varying functionalization conditions, while largely retaining the fiber geometry and flexibility. As schematically illustrated in **Figure 1a**, using the  $\text{MnO}_2$  coated fiber as positive electrode, the nitrogen-doped fiber as negative electrode, and a polymer gel as the electrolyte, a solid-state asymmetric micro-SC without binder, current collector, or separator was constructed. The optimized device can operate at a high-voltage of 1.8 V along with a long cycle life and good flexibility, and afford a remarkable volumetric energy density of  $5 \text{ mWh cm}^{-3}$ , higher than most of solid-state micro-SCs reported so far and even comparable to some thin film lithium batteries (or micro-batteries).

Both individual rGO and SWCNT fibers were previously reported;<sup>[9,22,23]</sup> however, their composite fibers have not yet been explored. Herein, our design is to firstly synthesize undoped rGO/SWCNT all-carbon composite fibers, which will be further functionalized by nitrogen-doping or  $\text{MnO}_2$  deposition for designing and fabricating suitable fiber electrodes. We firstly used nitric-acid-treated SWCNTs (about 1.4 nm in diameter) and GO (thickness of 0.7 nm and sizes ranging from several hundred nanometers to several micrometers, see Figure S1) to obtain all-carbon composite fibers through the hydrothermal

synthesis in a flexible fused silica column. The following synergistic effects are utilized in our process. First, SWCNTs exhibit excellent electrical conductivity, but limited electric double layer (EDL) capacitance.<sup>[24]</sup> In contrast, rGO sheets have large surface area for EDL capacitance but poor electrical conductivity.<sup>[4]</sup> The electrochemical properties of these two nanocarbon materials would complement each other in their composites.<sup>[25–28]</sup> Second, GO is a good surfactant to disperse SWCNTs, while SWCNTs hinder the restacking of GO sheets,<sup>[29]</sup> which makes it easy to prepare their homogenous aqueous suspension for the composite fiber formation. In a typical experiment, GO and SWCNT aqueous suspension at the optimal mass ratio was fed into the silica column. Then, the column was placed in an oven at 220  $^{\circ}\text{C}$  for 6.0 h with its two ends sealed. Afterwards, a continuous fiber was pushed into a water reservoir by pressurized nitrogen flow (Figure S2). The as-synthesized wet rGO/SWCNT fibers were further dried in air for 4.0 h, denoted as “GCF”. Figure 1b shows a 26-cm-long dried GCF fiber. It has a tensile strength of 88 MPa (Figure S3), comparable to that of wet-spun SWCNT fibers (50–150 MPa).<sup>[22]</sup> Scanning electron microscope (SEM) images (Figure 1c–f) show that the GCF fiber has an interconnected porous structure, different from that of the rGO fiber synthesized under the similar condition (Figure S4). Such interconnected network provides efficient conductive channels in the GCF fiber, as evidenced by the eight-fold increase in its electrical conductivity ( $\sim 100 \text{ S cm}^{-1}$ ), relative to that of the rGO fiber (Figure S5). More importantly, the GCF fiber shows excellent electrochemical properties (Figure S6) with a specific length capacitance up to  $\sim 1.5 \text{ mF cm}^{-1}$  at  $5 \text{ mV s}^{-1}$  in the 1.0 M  $\text{Na}_2\text{SO}_4$  electrolyte. This is 5-fold higher than that of the rGO fiber, and also much higher than those of most reported carbonaceous fibers, such as MWCNT fiber ( $0.015 \text{ mF cm}^{-1}$ ),<sup>[14]</sup> carbon fiber

(<0.1 mF cm<sup>-1</sup>),<sup>[10]</sup> and pen-ink-based fiber (0.504 mF cm<sup>-1</sup>).<sup>[8]</sup> The high specific capacitance of the SWCNT/rGO fiber can be attributed to its high electrical conductivity, relatively large Brunauer–Emmett–Teller specific surface area (368 m<sup>2</sup>/g) as well as a certain amount of oxygen-containing functionalities remained on the fiber (oxygen percentage: 12.8 at%, Figure S11), which can render not only good surface wettability (contact angle of 60°, Figure S7) but also more accessible electroactive surface area.<sup>[30]</sup> To date, a few carbonaceous fibers have been used for fiber-based capacitor electrodes. Common carbon fibers and CNT fibers, individually as electrodes, have high electrical conductivity but poor capacitive performance.<sup>[13,14]</sup> As a result, they are often used as conductive fibrous substrates to deposit other nanostructured materials (such as metal oxides and conductive polymers) to improve the overall capacitive performance. The rGO fiber is another emerging candidate, but it has poor electrical conductivity, undesirable as current collectors for charge transport.<sup>[9]</sup> Unlike these previously-reported carbonaceous fibers,<sup>[9,13,14]</sup> our flexible carbon composite fibers function as not only excellent active electrode materials but also current collectors, which provides an exceptional starting point to explore their applications in flexible micro-scale energy storage devices.

To convert the all-carbon composite fiber into a battery-type Faradic electrode (the positive electrode), the GCF fiber was used as a scaffold to deposit pseudocapacitive materials. MnO<sub>2</sub> is a pseudocapacitive material often used to fabricate asymmetric SCs.<sup>[6]</sup> It is known that carbon can reduce aqueous permanganate to obtain MnO<sub>2</sub> by the following reaction:<sup>[31]</sup>



The porous GCF fiber is hydrophilic (Figure S7), which facilitates the diffusion of MnO<sub>4</sub><sup>-</sup> ions in the fiber. Thus, we directly dipped the GCF fiber into the stirred 0.10 M KMnO<sub>4</sub>/0.10 M Na<sub>2</sub>SO<sub>4</sub> solution at room temperature for 5–30 min. The mass percentages of MnO<sub>2</sub> with different dipping times of 5, 10, 20 and 30 min are 7.25, 12.67, 17.02 and 19.56 wt%, respectively, which were determined by inductively coupled plasma-atomic emission spectrometry. X-ray diffraction analysis of the composite fiber indicates the approximately amorphous nature of the as-deposited MnO<sub>2</sub> particles due to lack of sharp peaks and broadening of peaks (Figure S8).<sup>[32]</sup> After dipping the GCF fiber for 10 min, the MnO<sub>2</sub>-coated GCF fiber (denoted as GCF/MnO<sub>2</sub>-10, Figure 2a–b) exhibits a different surface morphology compared to that of the GCF fiber (Figure 1d) with a thin layer of oxides coating on the carbon surface (Figure 2b). Elemental mapping analysis (Figure 2c) suggests a uniform distribution of Mn on the fiber together with C and O (Figure S9). X-ray photoelectron spectroscopy (XPS) spectra (Figures 2d and S10a) of the GCF/MnO<sub>2</sub>-10 fiber reveal that the binding energy of Mn 2p<sub>3/2</sub> and Mn 2p<sub>1/2</sub> appears at 654.2 and 642.4 eV, respectively, consistent with previous reported results, indicating the formation of manganese oxides.<sup>[33,34]</sup> The Mn 3s spectrum (Figure S10b) shows a peak separation value of 4.83 eV, suggesting that Mn<sup>4+</sup> is the dominant Mn species in the deposited manganese oxides.<sup>[31]</sup> The electrochemical characteristics of the GCF/MnO<sub>2</sub> fibers were evaluated by cyclic voltammetry (CV) at a scan rate of 10 mV s<sup>-1</sup> from 0 to 0.9 V in Na<sub>2</sub>SO<sub>4</sub> (1.0 M) electrolyte using a three-electrode configuration (Figure 2e). The potential window for manganese oxides is confined at 0–0.9 V versus SCE to avoid manganese dissolution at lower potentials and the oxygen evolution reaction at higher potentials.<sup>[18,32]</sup> The CV

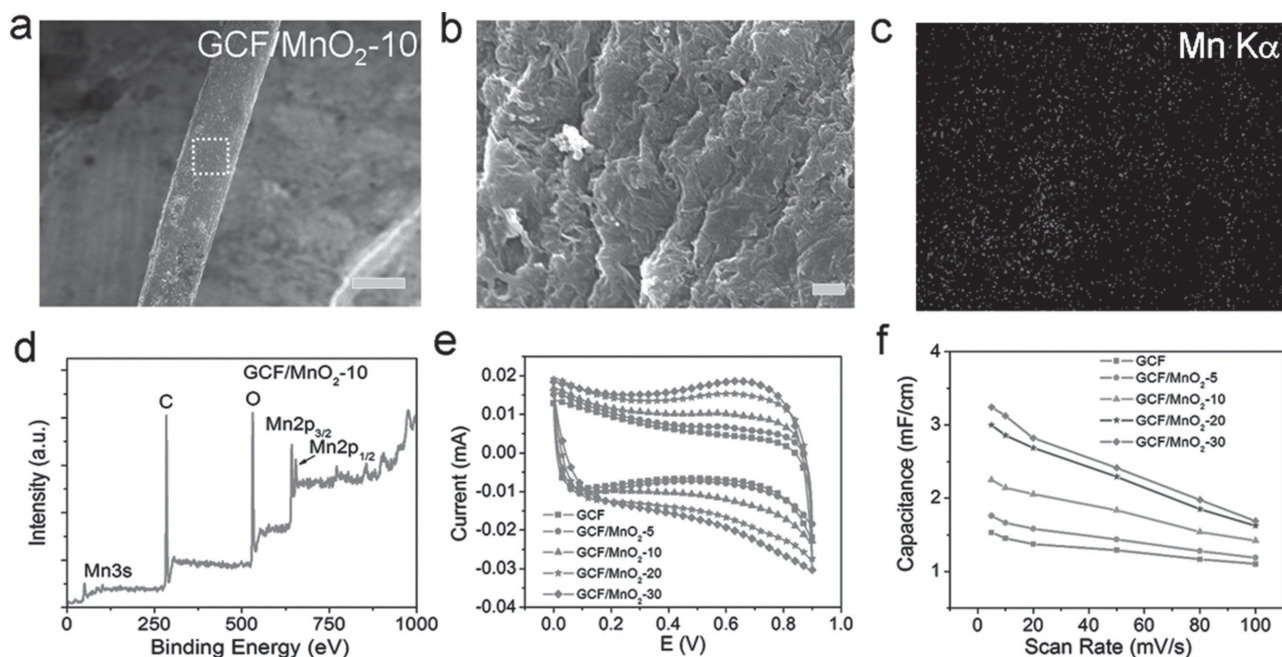


**Figure 2.** (a) The typical SEM image of the GCF/MnO<sub>2</sub>-10 fiber (scale bar: 50 μm); (b) high-magnification SEM image of the GCF/MnO<sub>2</sub>-10 fiber surface (scale bar: 100 nm); (c) Mn element mapping, corresponding to the square area highlighted in (a); (d) The wide survey XPS spectrum of the GCF/MnO<sub>2</sub>-10 fiber; (e) CV curves of individual GCF/MnO<sub>2</sub> fibers with different MnO<sub>2</sub> deposition time at the scan rate of 10 mV/s in aqueous 1.0 M Na<sub>2</sub>SO<sub>4</sub> electrolyte; (f) The specific length capacitance as a function of scan rate of different GCF/MnO<sub>2</sub> fibers.

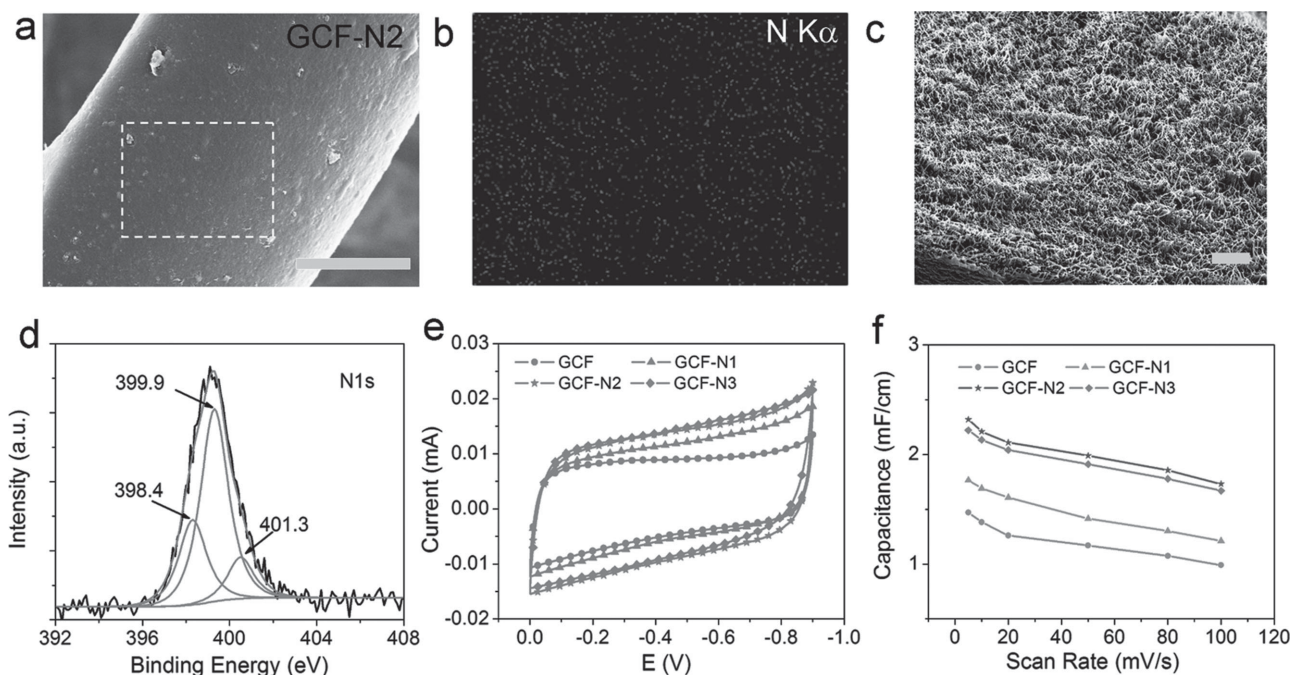


**Figure 3.** (a) The typical SEM image of the GCF-N2 fiber (scale bar: 20  $\mu\text{m}$ ); (b) N element mapping, corresponding to the square area highlighted in (a); (c) cross-sectional SEM image showing porous structure (scale bar: 1  $\mu\text{m}$ ); (d) High-resolution N1s XPS spectrum of the GCF-N2 fiber; (e) CV curves of individual GCF-N fibers with different doping at the scan rate of 10 mV/s in aqueous 1.0 M  $\text{Na}_2\text{SO}_4$  electrolyte; (f) The specific length capacitance as a function of scan rate for different GCF fibers.

curves of the GCF/ $\text{MnO}_2$  fibers display enlarging areas with the increase of the dipping time in the  $\text{KMnO}_4/\text{Na}_2\text{SO}_4$  solution. Since the diameter of the GCF fibers has minor changes before and after  $\text{MnO}_2$  deposition (Figure 1c and Figure 2a), we employed the specific length capacitance ( $\text{mF cm}^{-1}$ ) to evaluate the performance of the GCF/ $\text{MnO}_2$  fibers.<sup>[7]</sup> The capacitance of the GCF/ $\text{MnO}_2$  fibers surges from 1.5 (bare GCF fiber) to 1.76, 2.36, 3.01, and 3.30  $\text{mF cm}^{-1}$  at a scan rate of 5  $\text{mV s}^{-1}$  when the dipping time is prolonged from 0, 5, 10, 20, to 30 min, respectively. The higher capacitance of the deposited GCF fibers is attributed to the increasing amount of deposited pseudocapacitive  $\text{MnO}_2$ .<sup>[34]</sup> However, the rate capability of the GCF/ $\text{MnO}_2$  fibers deteriorates with the rise of the dipping time. The GCF/ $\text{MnO}_2$ -30 fiber retains only 53% of its capacitance when the scan rate increases from 5 to 100  $\text{mV s}^{-1}$ . This may result from the excessive  $\text{MnO}_2$  deposition at longer dipping time, blocking fast ion and charge transport. Further, the non-rectangular asymmetric CV curves observed from the GCF/ $\text{MnO}_2$ -30 fiber suggest electrode polarization. As suggested in the previous literatures on  $\text{MnO}_2/\text{CNT}$  composites,<sup>[35,36]</sup> this may be caused by the poor conductivity of thicker  $\text{MnO}_2$  coating layers. Nevertheless, the GCF fiber is demonstrated to be an excellent conductive template for  $\text{MnO}_2$  deposition, resulting in novel Faradic fiber electrodes with tunable capacitances without significant changes in geometry or mechanical properties (Figure S3).

Subsequently, we created a capacitor-type electrode (the negative electrode) from the rGO/SWCNT all-carbon fiber. Our recent finding suggests that nitrogen-doped carbon nanomaterials are excellent negative electrode materials for high-performance asymmetric capacitors with high operating voltage.<sup>[37]</sup> Our strategy in this work is to dope nitrogen into rGO/SWCNT

all-carbon fiber to enhance its electrochemical capacitive performance while largely preserving its flexibility and geometry. To synthesize N-doped composite fibers, urea was introduced in the aqueous mixture of GO and SWCNTs to obtain the starting precursor, followed by the hydrothermal treatment in the flexible fused silica column. Under hydrothermal conditions, urea can serve as an effective nitrogen source to dope graphene materials, as demonstrated in our previous work.<sup>[38]</sup> By varying the mass ratio between urea, GO and SWCNTs from 1:1:1, 2:1:1, to 4:1:1, three nitrogen doped fibers were produced, which are denoted as GCF-N1, GCF-N2, and GCF-N3, respectively. Figure 3a,c shows the typical SEM images of the GCF-N2 fiber, which reveal similar geometry size ( $\sim 47 \mu\text{m}$  in diameter) and porous structure as that of the undoped GCF fiber (Figure 1c and 1e). The elemental mapping of the GCF-N2 fiber (Figure 3b) reveals uniform doping of nitrogen. Compared to that of the undoped GCF fiber, the XPS spectrum of the GCF-N2 fiber (Figure S11) presents an additional nitrogen peak with the nitrogen content of 3.15 at% (Table S1), which is higher than those of GCF-N1 (1.23 at%) and GCF-N3 (2.72 at%). The high-resolution N1s spectrum (Figure 3d) can be divided into several types of N functional groups: the 398.4 eV peak is attributed to the pyridinic N, the 399.9 eV peak corresponds to the pyrrolic N, and the 401.3 eV peak is assigned to the graphitic N.<sup>[38]</sup> The capacitance of GCF fibers was enhanced after nitrogen doping. It is evidenced by the comparative CV profiles at the same scan rate of 10  $\text{mV s}^{-1}$  in a three-electrode cell using 1.0 M  $\text{Na}_2\text{SO}_4$  aqueous electrolyte (Figure 3e), which reveals that the areas for the N-doped GCF fibers are much larger than that of the undoped GCF fiber. Among all doped GCF fibers investigated in this work, the GCF-N2 fiber has the largest

specific length capacitance of  $2.37 \text{ mF cm}^{-1}$  at a scan rate of  $5 \text{ mV s}^{-1}$ , substantially higher than that of the undoped GCF fiber ( $\sim 1.5 \text{ mF cm}^{-1}$ ), which can be attributed to the highest conductivity and nitrogen-doping level of the GCF-N2 (Table S1). The corresponding specific volumetric capacitance of  $\sim 137 \text{ F cm}^{-3}$  (see calculation methods in the supporting information) in  $\text{Na}_2\text{SO}_4$  for the GCF-N2 fiber derived from urea is comparable to our recent reported N-doped carbon composite fiber derived from EDA as the nitrogen source in a neutral electrolyte ( $\text{LiClO}_4$ ).<sup>[21]</sup> Furthermore, the GCF-N2 fiber also exhibits excellent rate capability with a capacitance retention of 73% when the scanning rate increases from 5 to  $100 \text{ mV s}^{-1}$ , higher than that of the undoped GCF fiber. The improved electrochemical performance of the GCF-N2 fiber can be ascribed to efficient doping of suitable nitrogen species.<sup>[37,39,40]</sup> Nitrogen doping can enhance the capacitance of carbon materials through three ways.<sup>[39]</sup> First, nitrogen doping can improve the surface wettability of carbon materials, resulting in an increase of electrolyte accessible surface area, which facilitates the formation of EDL.<sup>[39a]</sup> Second, the graphitic-N may enhance the conductivity of carbon materials, expediting charge transport.<sup>[39b-c]</sup> Third, the pyridinic-N and pyrrolic-N may provide pseudocapacitance by some redox reactions in acidic or basic electrolytes.<sup>[39d]</sup> Here, the fibers were characterized in the neutral  $\text{Na}_2\text{SO}_4$  electrolyte. Because neutral electrolytes contain balanced numbers of hydrogen and hydroxide ions, the redox reaction induced by the pyridinic-N and pyrrolic-N species are largely suppressed.<sup>[39e]</sup> Thus, we propose that the observed capacitance enhancement by nitrogen doping mainly comes from the first two ways mentioned above.

Next, we fabricated high-voltage asymmetric solid-state micro-SCs using the  $\text{MnO}_2$  coated GCF fiber as positive electrode and nitrogen doped GCF fiber as negative electrode, as illustrated in Figure 4a. Two types of fiber electrodes with the identical length were mounted on a flexible polyester (PET) substrate using polyvinylpyrrolidone (PVP)- $\text{Na}_2\text{SO}_4$  gelled electrolyte<sup>[41]</sup> without binders, current collectors, separator, and any other packaging materials. Apart from serving as the electrolyte, the gel also works as an effective separator to prevent the undesirable short circuit of the two electrodes.<sup>[21,41]</sup> Such design avoids the possible harmful leakage of conventional liquid electrolytes, decreases the device volume and simplifies fabrication process. It should be noted that acidic electrolytes were used in our previous study.<sup>[21]</sup> However,  $\text{MnO}_2$  in the positive electrode is not stable in acidic environment, thus the neutral  $\text{Na}_2\text{SO}_4$  electrolyte was used in the asymmetric device in this study. Moreover, the neutral gel electrolyte is safer for potential applications of practical wearable devices. Figure 4b shows that the potential windows of the N-doped GCF and GCF/ $\text{MnO}_2$  electrodes are  $-0.9-0 \text{ V}$  and  $0-0.9 \text{ V}$ , respectively. Thus, it is anticipated that the maximum operation potential for the proposed asymmetric micro-SC can reach 1.8 V. In order to obtain the maximum performance of the asymmetric cell, a critical issue is to achieve charge balance between the positive and negative electrodes, which follows the relationship  $Q^+ = Q^-$ .<sup>[6]</sup> Because our active fiber electrodes have unique 1D architecture and small mass, we employ "capacitance per unit length", instead of gravimetric capacitance commonly used in conventional macro-scale SCs, to characterize the capacitance behavior of

two fiber electrodes and adjust the charge balance between two active electrodes.<sup>[7]</sup> The charge stored by each electrode depends on the specific length capacitance ( $C_L$ ), the potential window for the charge/discharge process ( $\Delta E$ ) and the length of the electrode ( $L$ ) following the Equation (1):

$$Q = C_L \times \Delta E \times L \quad (1)$$

and in order to obtain  $Q^+ = Q^-$ , the device parameters should meet the following Equation (2):

$$L^+ / L^- = C_L^- \times \Delta E^- / C_L^+ \times \Delta E^+ \quad (2)$$

Considering that the length and the potential window for the N-doped GCF and GCF/ $\text{MnO}_2$  fiber electrodes are the same in the proposed device (Figure 4a-b), according to Equation (2), two type of fiber electrodes have same capacitance. The GCF-N2 fiber has the highest specific capacitance at  $2.37 \text{ mF cm}^{-1}$  and the best rate capability among all N-doped GCF fibers synthesized in this work, thus it is employed as the negative electrode. To match the negative electrode, the GCF/ $\text{MnO}_2$ -10 fiber with a specific capacitance of  $2.36 \text{ mF cm}^{-1}$  was selected as the positive electrode.

Figure 4c shows the CV profiles of the GCF-N2//GCF/ $\text{MnO}_2$ -10 asymmetric micro-SC at the scan rate of  $10 \text{ mV s}^{-1}$  in different potential windows. Clearly, the asymmetric device presents rectangular-like CV curves even at a high potential window up to 1.8 V, which is about twice as high as those of recently reported symmetric solid-state micro-SCs ( $0.8-1\text{V}$ ).<sup>[7-17,21]</sup> Figure S12 exhibits its CV curves at different scan rates from 5 to  $200 \text{ mV s}^{-1}$ . The CV profiles keep rectangular-like shape even at a higher scan rate of  $200 \text{ mV s}^{-1}$ , manifesting its excellent capacitive behavior. Furthermore, the galvanostatic charge/discharge curves of the micro-SC at  $250 \text{ mA cm}^{-3}$  are shown in Figure 4d. Its discharge curves offer nearly linear variation with the cell potential. The volumetric capacitance of the asymmetric cell (normalized to the device volume including two fibers and the surrounding electrolyte) at different charge/discharge rates was calculated based on the charge/discharge curves. The volumetric capacitance of the micro-SC is  $\sim 11.1 \text{ F cm}^{-3}$  at  $\sim 25 \text{ mA cm}^{-3}$  and retains  $\sim 5.2 \text{ F cm}^{-3}$  at  $\sim 1000 \text{ mA cm}^{-3}$ , indicating good rate capability. The mass of active materials is very small in microscale energy storage devices, thus the volumetric power/energy densities are more reliable performance metrics for micro-SCs compared with gravimetric power/energy densities.<sup>[21,42]</sup> The Ragone plot (Figure 4f) compares the volumetric performance of the asymmetric micro-SC in this work with those of commercially available energy-storage devices. The asymmetric micro-SC has a maximum volumetric energy density (normalized to the device volume) of  $\sim 5 \text{ mWh cm}^{-3}$ , which is about 8 folds higher than those of typical bulk SCs ( $2.75\text{V}/44\text{-mF}$  and  $5.5\text{V}/100\text{-mF}$ ,  $< 1 \text{ mWh/cm}^{-3}$ ) and even comparable to the  $4\text{V}/500\text{-}\mu\text{Ah}$  thin-film lithium battery ( $0.3-10 \text{ mWh/cm}^{-3}$ ). The energy density value calculated based on the device volume is much higher than most reported carbon-based solid-state symmetric micro-SCs ( $0.8-1\text{V}$ ) in the format of either thin films or fibers (Table S2),<sup>[1-4,7,9-15,17,43-46]</sup> such as the CNT/carbon fiber coaxial micro-SC ( $0.14 \text{ mWh cm}^{-3}$ , PVA/ $\text{H}_3\text{PO}_4$ ),<sup>[10]</sup>  $\text{MnO}_2$  coated

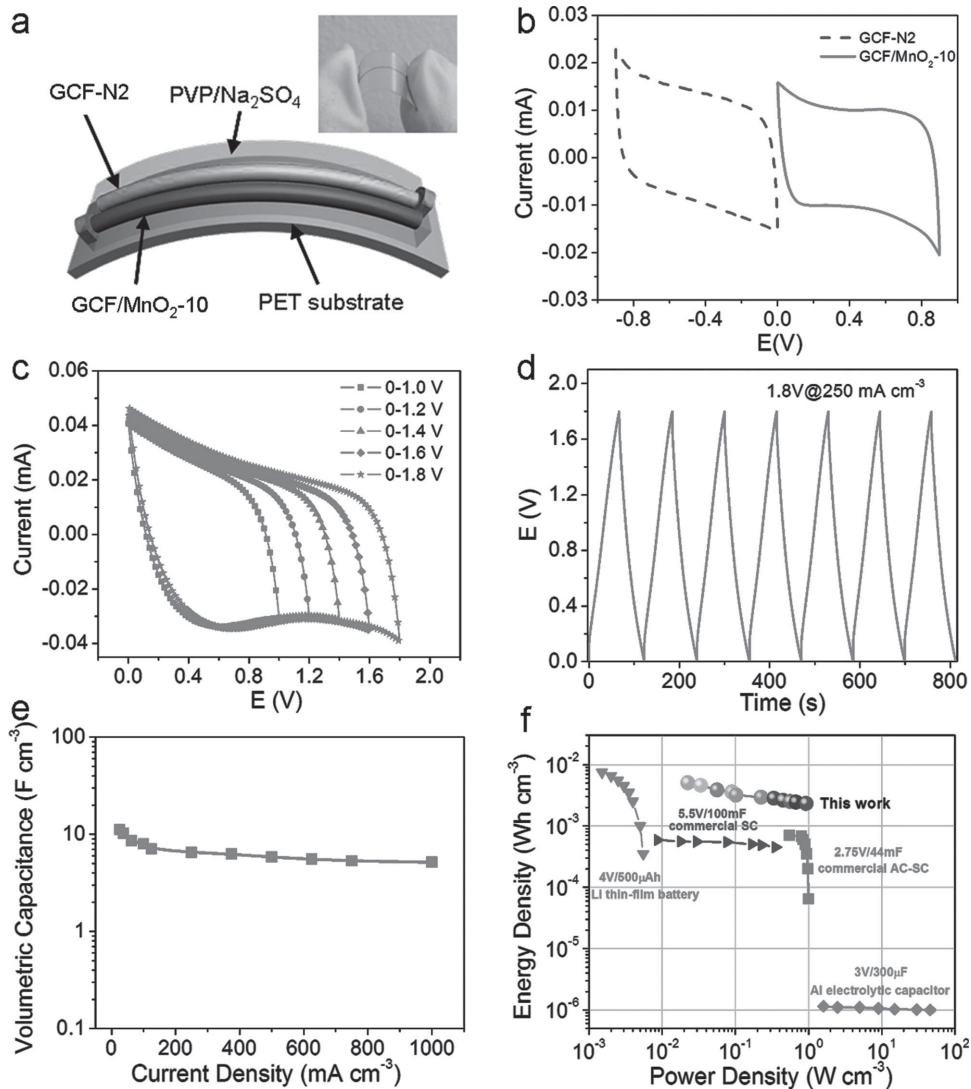


**Figure 4.** (a) Schematic illustration and photo of an asymmetric micro-SC constructed using the GCF-N2 fiber as the negative electrode and the GCF/MnO<sub>2</sub>-10 fiber as the positive electrode. (b) Comparative CV curves obtained for the GCF-N2 and GCF/MnO<sub>2</sub>-10 fibers at the scan rate of 10 mV s<sup>-1</sup>. (c) CV curves of the asymmetric GCF-N2//GCF/MnO<sub>2</sub>-10 micro-SC with different operation voltages at the scan rate of 50 mV s<sup>-1</sup>. (d) Galvanostatic charge-discharge curves of the asymmetric GCF-N2//GCF/MnO<sub>2</sub>-10 micro-SC at 250 mA cm<sup>-3</sup>. (e) The volumetric capacitance normalized to the device volume at different current densities. (f) The energy and power densities of the micro-SC compared with commercially available energy-storage systems. Data of the Li battery are from Ref. [1] and data of the 2.75V/44 mV activated carbon (AC)-SC are reproduced from Ref. [3].

carbon fiber-based micro-SC (0.22 mWh cm<sup>-3</sup>, PVA/H<sub>3</sub>PO<sub>4</sub>),<sup>[13]</sup> PEDOT/CNT/Pt wire-based micro-SC (1.4 mWh cm<sup>-3</sup>, PVA/H<sub>2</sub>SO<sub>4</sub>),<sup>[45]</sup> graphene-based in plane micro-SC (2.5 mWh cm<sup>-3</sup>, PVA/H<sub>2</sub>SO<sub>4</sub>),<sup>[46]</sup> It is even better than those of some micro-devices calculated only using the volume of active electrodes (Table S2) like activated carbon@SWCNT yarn-based micro-SC (3.7 mWh cm<sup>-3</sup>, PVA/H<sub>2</sub>SO<sub>4</sub>)<sup>[47]</sup> and MWCNT-rGO@cellulose composite yarn-based micro-SC (3.5 mWh cm<sup>-3</sup>, PVA/H<sub>3</sub>PO<sub>4</sub>),<sup>[48]</sup> Moreover, the energy density value is about seven-fold higher than that of recently reported asymmetric device based on Co<sub>3</sub>O<sub>4</sub>/metal fibers @ graphene/carbon fibers (1.5 V, 0.62 mWh cm<sup>-3</sup>, PVA/KOH).<sup>[49]</sup> This is because that metal fibers as current collectors, unlike our composite fibers, did not contribute to store energy but account for a considerable volume portion of the whole device, which inevitably increases the total

volume of the device and thus compromises the volumetric energy density. Our device also exhibits the high volumetric power density of ~929 mW cm<sup>-3</sup>, which is comparable to typical commercially available SCs, and about two orders higher than that of thin film lithium batteries (Figure 4f).<sup>[1,3]</sup>

We proposed that the following factors could contribute to the excellent performances of the asymmetric micro-SCs: (1) both fiber electrodes have large specific capacitances; (2) the asymmetric device are operated at a high cell voltage up to 1.8 V; (3) the device design only using two fibers and the gel electrolyte without binders, current collectors, separators, or other packing materials significantly reduces the total volume of the device; and (4) the synergy between the positive and negative electrodes enhance both energy and power density. The MnO<sub>2</sub> coated GCF fibers afford pseudocapacitive materials for

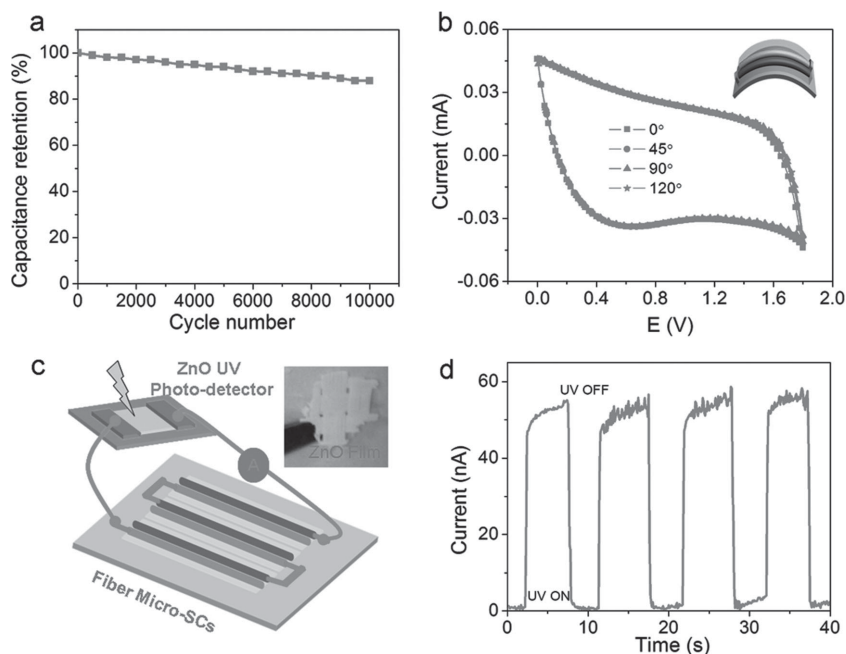


**Figure 5.** (a) Cycle life of the asymmetric GCF-N2//GCF/MnO<sub>2</sub>-10 micro-SC; (b) CV curves of one asymmetric micro-SC, which are bended at different angles; (c) Schematic illustration of a self-powered nanosystem, and the inset is the optical image of a ZnO film; (d) Current response of the UV photodetector based on the ZnO powered by multiple micro-SCs connected in series.

reversible Faradic reaction, while the N-doped GCF fibers provide faster electron transfer.

We further tested the stability and flexibility of the assembled device. **Figure 5a** shows that the micro-SC retains 87% of its initial capacity after 10,000 charge-discharge cycles under the current density of 200 mA cm<sup>-3</sup>, indicating long cycle life, as is the case for previously reported asymmetric macro-scale SCs based on amorphous MnO<sub>2</sub> materials.<sup>[50]</sup> In addition, the TEM images of the GCF/MnO<sub>2</sub> electrode materials (**Figure S13**) before and after 10 000 cycles show no obvious morphology changes. **Figure 5b** presents CV curves of the micro-SC under different bending angles (0°, 45°, 90°, and 120°). All CV curves show similar capacitive behavior with minor capacitance changes (<0.05%), demonstrating excellent flexibility. To further demonstrate its potential applications as efficient energy storage components for electronic and optoelectronic devices, a self-powered nanosystem was constructed, in which three fully-charged micro-SC were connected in series to power a ZnO film based UV photodetector without any external bias voltage (**Figure 5c**). The ZnO film was prepared using a previously reported hydrothermal method.<sup>[51]</sup> **Figure 5d** shows that the UV photodetector has substantial responses to UV light irradiation ( $\lambda = 365$  nm).

In summary, we have demonstrated the synthesis and controllable functionalization of rGO/SWCNT all-carbon fibers by a facile and effective method, yielding versatile fibers with either capacitive or Faradic characteristics for designing high-performance asymmetric fiber micro-SCs. The capacitive-type N-doped rGO/SWCNT fibers obtained through in situ N-doping with urea in the flexible capillary column show tunable specific capacitances from 1.75 to 2.37 mF cm<sup>-1</sup>, while the Faradic-type fibers created by redox deposition of MnO<sub>2</sub> on the rGO/SWCNT

fibers have specific capacitances ranging from 1.76 to 3.30 mF cm<sup>-1</sup>. Both types of functionalized fibers outperform the pristine rGO/SWCNT fibers (1.5 mF cm<sup>-1</sup>), while retaining fiber geometry and mechanical flexibility. By matching the specific capacitances of one MnO<sub>2</sub>-coated rGO/SWCNT fiber as battery-type (positive) electrode and the other N-doped rGO/SWCNT fiber as capacitor-type (negative) electrode to achieve the charge balance between two fiber electrodes, we designed and constructed the fiber-based solid-state asymmetric micro-SC with polymer gelled neutral electrolyte on a flexible polymer substrate. The optimized device exhibits a stable and high voltage window of 1.8 V and excellent cycling stability (87% capacitance retention after 10 000 cycles), as well as good flexibility. More importantly, the device delivers a high volumetric energy density of ~5 mWh cm<sup>-3</sup>, superior to most reported solid-state micro-SCs to date and even comparable to the 4V/500- $\mu$ Ah thin-film lithium battery, while its power density of 929 mW cm<sup>-3</sup> is comparable to typical commercially activated carbon SCs and about two orders higher than that of thin film lithium batteries. This facile design and rational syn-

thesis open an avenue to fabricate high-performance fibrous micro-scale energy storage devices and our developed fiber-based asymmetric micro-SC with high operation voltage and remarkable volumetric energy density have great potentials in flexible and portable electronics, as exemplified by powering a ZnO based UV photodetector in this study. Furthermore, the applications of the newly-developed various composite fibers are not limited to advanced electrode materials for micro-SCs, they have much broader potentials for functional textile, smart cloths, flexible electronics, sensors, as well as biofuel cells.

## Supporting Information

Supporting Information is available from the Wiley Online Library or from the author.

## Acknowledgements

This work was supported by Ministry of Education, Singapore (MOE2011-T2-2-062 and 2013-T1-002-132), and Asian Office of Aerospace Research and Development of the U.S. Air Force (FA23861314110).

Received: July 9, 2014

Revised: August 2, 2014

Published online: September 2, 2014

[1] D. Pech, M. Brunet, H. Durou, P. Huang, V. Mochalin, Y. Gogotsi, P. L. Taberna, P. Simon, *Nat. Nanotechnol.* **2010**, *5*, 651.

[2] W. Gao, N. Singh, L. Song, Z. Liu, A. L. M. Reddy, L. Ci, R. Vajtai, Q. Zhang, B. Wei, P. M. Ajayan, *Nat. Nanotechnol.* **2011**, *6*, 496.

- [3] M. F. El-Kady, R. B. Kaner, *Nat. Commun.* **2013**, *4*, 1475.
- [4] J. Lin, C. G. Zhang, Z. Yan, Y. Zhu, Z. W. Peng, R. H. Hauge, D. Natelson, J. M. Tour, *Nano Lett.* **2013**, *13*, 72.
- [5] X. H. Lu, M. H. Yu, T. Zhai, G. M. Wang, S. L. Xie, T. Y. Liu, C. L. Liang, Y. X. Tong, Y. Li, *Nano Lett.* **2013**, *13*, 2628.
- [6] Z. S. Wu, W. Ren, D. W. Wang, F. Li, B. Liu, H. M. Cheng, *ACS Nano* **2010**, *4*, 5835.
- [7] J. Bae, M. K. Song, Y. J. Park, J. M. Kim, M. Liu, Z. L. Wang, *Angew. Chem. Int. Ed.* **2011**, *50*, 1683.
- [8] Y. Fu, X. H. Cai, Z. Lv, S. Hou, M. Peng, X. Yu, D. Zou, *Adv. Mater.* **2012**, *24*, 5713.
- [9] Y. Meng, Y. Zhao, C. Hu, H. Cheng, Y. Hu, Z. Zhang, G. Shi, L. Qu, *Adv. Mater.* **2013**, *25*, 2326.
- [10] V. T. Lee, H. Kim, A. Ghosh, J. Kim, Jian Chang, Q. A. Vu, D. T. Pham, J. H. Lee, S. W. Kim, Y. Lee, *ACS Nano* **2013**, *7*, 5940.
- [11] X. Chen, L. Qiu, J. Ren, G. Guan, H. Lin, Z. Zhang, P. Chen, Y. Wang, H. Peng, *Adv. Mater.* **2013**, *25*, 6436.
- [12] J. Ren, W. Bai, G. Guan, Y. Zhang, H. Peng, *Adv. Mater.* **2013**, *25*, 5965.
- [13] X. Xiao, T. Li, P. Yang, Y. Gao, H. Jin, W. Ni, W. Zhan, X. Zhang, Y. Cao, J. Zhong, L. Gong, W. Yen, W. Mai, J. Chen, K. Huo, Y. Chueh, Z. Wang, J. Zhou, *ACS Nano* **2012**, *6*, 9200.
- [14] J. Ren, L. Li, C. Chen, X. Chen, Z. Cai, L. Qiu, Y. Wang, X. Zhu, H. Peng, *Adv. Mater.* **2012**, *25*, 1155.
- [15] K. Wang, Q. Meng, Y. Zhang, Z. Wei, M. Miao, *Adv. Mater.* **2013**, *25*, 1494–1498.
- [16] J. Tao, N. Liu, W. Ma, L. Ding, L. Li, J. Su, Y. Gao, *Sci. Rep.* **2013**, *3*, 2286.
- [17] N. Liu, W. Ma, J. Tao, X. Zhang, J. Su, L. Li, C. Yang, Y. Gao, D. Golberg, Y. Bando, *Adv. Mater.* **2013**, *25*, 4925.
- [18] Z. Fan, J. Yan, T. Wei, L. Zhi, G. Ning, T. Li, F. Wei, *Adv. Funct. Mater.* **2011**, *21*, 2366.
- [19] P. C. Chen, G. Shen, Y. Shi, H. Chen, C. Zhou, *ACS Nano* **2010**, *4*, 4403.
- [20] J. Yan, Z. Fan, W. Sun, G. Ning, T. Wei, Q. Zhang, R. Zhang, L. Zhi, F. Wei, *Adv. Funct. Mater.* **2012**, *22*, 2632.
- [21] D. S. Yu, K. Goh, H. Wang, L. Wei, Q. Zhang, L. Dai, Y. Chen, *Nature Nanotech.* **2014**, *9*, 555.
- [22] H. P. Cong, X. C. Ren, P. Wang, S. H. Yu, *Sci. Rep.* **2012**, *2*, 613.
- [23] W. Lu, M. Zu, J. H. Byun, B. S. Kim, T. W. Chou, *Adv. Mater.* **2012**, *24*, 1805.
- [24] Y. Li, Z. Li, P. Shen, *Adv. Mater.* **2013**, *25*, 2474.
- [25] D. S. Yu, L. Dai, *J. Phys. Chem. Lett.* **2010**, *1*, 467.
- [26] F. Du, D. S. Yu, L. M. Dai, S. Ganguli, V. Varshney, A. K. Roy, *Chem. Mater.* **2011**, *23*, 4810.
- [27] N. Jha, P. Ramesh, E. Bekyarova, M. E. Itkis, R. C. Haddon, *Adv. Energy Mater.* **2012**, *2*, 438.
- [28] M. Q. Zhao, X. F. Liu, Q. Zhang, G. L. Tian, J. Q. Huang, W. C. Zhu, F. Wei, *ACS Nano* **2012**, *6*, 10759.
- [29] L. J. Cote, J. Kim, V. C. Tung, J. Luo, F. Kim, J. Huang, *Pure Appl. Chem.* **2011**, *83*, 201195.
- [30] J. Yan, Q. Wang, T. Wei, L. Jiang, M. Zhang, X. Jing, Z. Fan, *ACS Nano* **2014**, *8*, 4720.
- [31] S. W. Lee, J. Kim, S. Chen, P. T. Hammond, Y. Shao-Horn, *ACS Nano* **2010**, *4*, 3889.
- [32] J. Cao, Y. Wang, Y. Zhou, J. Ouyang, D. Jia, L. Guo, *J. Electroanal. Chem.* **2013**, *689*, 201.
- [33] M. Toupin, T. Brousse, D. Bélanger, *Chem. Mater.* **2004**, *16*, 3184.
- [34] D. G. Ivey, W. F. Wei, X. W. Cui, W. X. Chen, *Chem. Soc. Rev.* **2011**, *40*, 1697.
- [35] F. Teng, S. Santhanagopalan, Y. Wang, D. D. Meng, *J. Alloys Comp.* **2010**, *499*, 259.
- [36] M. Toupin, T. Brousse, D. Bélanger, *Chem. Mater.* **2002**, *14*, 3946.
- [37] D. S. Yu, K. Goh, L. Wei, H. Wang, Q. Zhang, W. Jiang, R. Si, Y. Chen, *J. Mater. Chem. A* **2013**, *1*, 11061.
- [38] D. S. Yu, L. Wei, W. Jiang, H. Wang, B. Sun, Q. Zhang, K. Goh, R. Si, Y. Chen, *Nanoscale* **2013**, *5*, 3457.
- [39] a) G. Lota, B. Grzyb, H. Machnikowska, J. Machnikowski, E. Frackowiak, *Chem. Phys. Lett.* **2005**, *404*, 53; b) H. M. Jeong, J. W. Lee, W. H. Shin, Y. J. Choi, H. J. Shin, J. K. Kang, J. W. Choi, *Nano Lett.* **2011**, *11*, 2472; c) L. Sun, L. Wang, C. Tian, T. Tan, Y. Xie, K. Shi, M. Li, H. Fu, *RSC Adv.* **2012**, *2*, 4498; d) Y. H. Lee, K. H. Chang, C. C. Hu, *J. Power Sources* **2013**, *227*, 300; e) D. Kang, J. H. Moon, *Sci. Rep.* **2014**, *4*, 5392.
- [40] D. Hulicova-Jurcakova, M. Kodama, S. Shiraishi, H. Hatori, Z. H. Zhu, G. Q. Lu, *Adv. Funct. Mater.* **2009**, *19*, 1800.
- [41] Y. Jin, H. Chen, M. Chen, N. Liu, Q. Li, *ACS Appl. Mater. Interfaces* **2013**, *5*, 3408.
- [42] X. Yang, C. Cheng, Y. Wang, L. Qiu, D. Li, *Science* **2013**, *341*, 543.
- [43] W. Liu, Y. Feng, J. Chen, Q. Xue, *Adv. Funct. Mater.* **2013**, *23*, 4111.
- [44] M. Beidaghi, C. Wang, *Adv. Funct. Mater.* **2012**, *22*, 4501.
- [45] J. A. Lee, M. K. Shin, S. H. Kim, H. U. Cho, G. M. Spinks, G. G. Wallace, M. D. Lima, X. Lepro, M. E. Kozlov, R. H. Baughman, S. J. Kim, *Nat. Commun.* **2013**, *4*, 1970.
- [46] Z. Wu, K. Parvez, X. Feng, K. Mullen, *Nat. Commun.* **2013**, *4*, 2487.
- [47] Q. Meng, H. Wu, Y. Meng, K. Xie, Z. Wei, Z. Guo, *Adv. Mater.* **2014**, *26*, 4100.
- [48] L. Kou, T. Huang, B. Zheng, Y. Han, X. Zhao, K. Gopalsamy, H. Sun, C. Gao, *Nat. Commun.* **2014**, *5*, 3754.
- [49] X. Wang, B. Liu, R. Liu, Q. Wang, X. D. Chen, R. Wang, G. Shen, *Angew. Chem. Int. Ed.* **2014**, *53*, 1849.
- [50] Q. Qu, P. Zhang, B. Wang, Y. Chen, S. Tian, Y. Wu, R. Holze, *J. Phys. Chem. C* **2009**, *113*, 14020.
- [51] B. Liu, Z. R. Wang, Y. Dong, Y. G. Zhu, Y. Gong, S. H. Ran, Z. Liu, J. Xu, Z. Xie, D. Chen, G. Shen, *J. Mater. Chem.* **2012**, *22*, 9379.